

Super-Resolution Bright-Field Optical Microscopy Based on Nanometer Topographic Contrast

SHU-WEI HUANG,¹ HONG-YAO MONG,² AND CHAU-HWANG LEE^{2*}

¹Department of Electrical Engineering, National Taiwan University, Taipei 106, Taiwan

²Research Center for Applied Sciences, Academia Sinica, Taipei 115, Taiwan

KEY WORDS image restoration; nanometer depth resolution; wide-field optical profilometer

ABSTRACT By using an expectation-maximization maximum likelihood estimation algorithm to improve the lateral resolution of a recently developed non-interferometric wide-field optical profilometer, we obtain super-resolution bright-field optical images of nanometer features on a flat surface. The optical profilometer employs a 365-nm light source and an ordinary objective lens of a 0.95 numerical aperture. For objects of 100 nm thickness, lateral features about $\lambda/7$ can be resolved in the restored images without fluorescence labeling. Current image acquisition rate is 0.1 frame/sec, which is limited by the brightness of the light source. With a brighter light source, the imaging speed can be fast enough for real-time observation of dynamic activities in the nanometer scale. *Microsc. Res. Tech.* 65:180–185, 2004. © 2005 Wiley-Liss, Inc.

INTRODUCTION

Bright-field optical microscopy is the most convenient technique for observing microscopic phenomena. However, the simple contrast mechanism limits its applications to observing samples with large variance of absorption or reflectivity. Modern resolution enhancing techniques for fluorescence microscopy (Carrington et al., 1995; Frohn et al., 2000; Gustafsson, 2000; Klar and Hell, 1999; Schrader et al., 1996) are difficult to apply on bright-field microscopy because they usually require the high contrast from fluorescent dyes. Other contrast mechanisms have been employed, including phase contrast and differential interference contrast, and the improvement on the versatility of bright-field optical microscopy is tremendous. Quantitative profiling techniques for transparent objects based on phase measurement have also been developed (Barty et al., 1998). Nevertheless, the above methods do not enhance the lateral resolution. Even the image-restoration techniques for fluorescence microscopy can hardly be applied on the phase contrast and differential interference contrast techniques because the contrast originates from the phase difference and gradients, which are not well-defined for objects of lateral dimensions smaller than a wavelength. One can also improve the resolution of scanning microscopy by adding binary or holographic masks into the detecting optical path to modify the point-spread function (PSF) (Akduman et al., 1998; Walker et al., 1993). However, the design and fabrication of such masks could be complicated, especially for coherent imaging with high numerical apertures (NAs).

Recently, we demonstrated an idea for improving the lateral resolution of far-field optical microscopy by using an image restoration algorithm to process images of nanometer topographic contrast (Lee et al., 2003). The contrast was from a far-field optical profiling technique called differential confocal microscopy (DCM) (Lee and Wang, 1997; Tsai et al., 1999). Working in the sharp linear region of the axial response curve of confocal

microscopy, DCM provides depth resolution of a few nanometers with a conventional objective lens and a visible light source. Relying on the nanometer depth sensitivity, on a flat surface DCM can detect the blurred shapes of nanometer-high objects with lateral features smaller than the diffraction limit. As long as the signal-to-noise ratio is high enough, the lateral resolution can be enhanced by image-restoration algorithms. We achieved lateral resolution ~ 80 nm when the sample was illuminated by a 532-nm light source and the reflected signal light was collected by an objective lens of a 0.95 NA. Nevertheless, DCM is a scanning profiling technique. For a medium-size frame, e.g., 256×256 pixels, image acquisition time longer than one minute is usually required for a sufficiently high signal-to-noise ratio. This character makes super-resolution DCM useful only for observing static specimens.

In this article, we demonstrate a new scheme that can obtain super-resolution bright-field images based on the topographic contrast with an image-acquisition speed potentially capable of real-time display. The topographic contrast is provided by a non-interferometric wide-field optical profilometer (NIWOP), which operates in the sharp linear range of the axial response curve of wide-field optically sectioning microscopy (Neil et al., 1997). With our homemade NIWOP, 2-nm depth resolution has been demonstrated by using the 550-nm light from a power-regulated tungsten lamp as the illumination and a 14-bit CCD camera as the detector (Lee et al., 2002). Because the image frame is taken in a parallel way within a few seconds of exposure time,

*Correspondence to: Dr. Chau-Hwang Lee, Research Center for Applied Sciences, Academia Sinica, 128 Sec. 2, Academia Rd., Nankang, Taipei 115, Taiwan. E-mail: cleee@gate.sinica.edu.tw

Received 16 July 2004; accepted in revised form 24 August 2004

Contract grant sponsor: National Science Council of Taiwan; Contract grant number: NSC 92-2112-M-001-055.

DOI 10.1002/jemt.20091

Published online in Wiley InterScience (www.interscience.wiley.com).

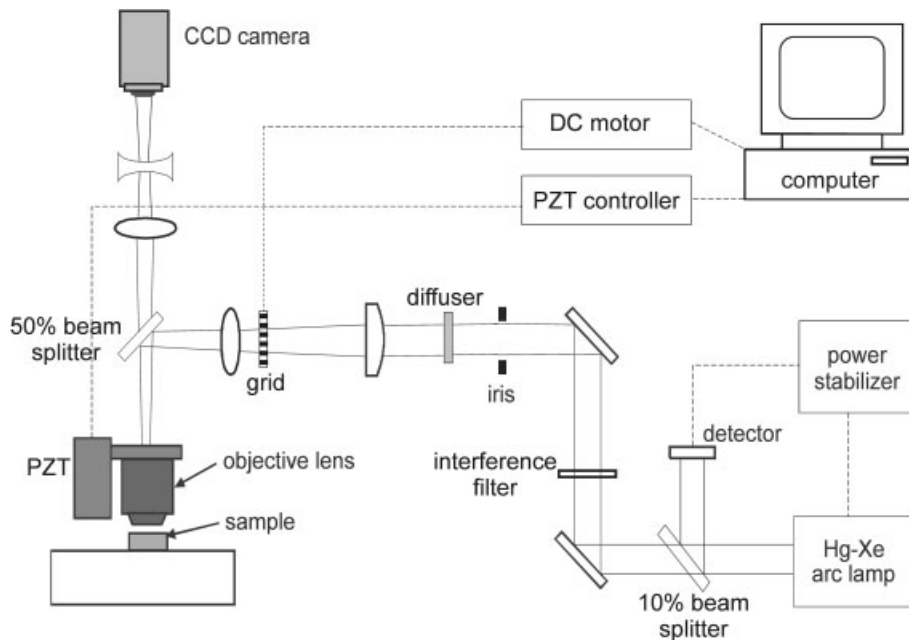


Fig. 1. Setup of the non-interferometric wide-field optical profilometer (NIWOP). Solid lines represent the light paths, while dashed lines are the electrical wiring.

this technique is suitable for observing morphological variations of nanometric features.

MATERIALS AND METHODS

Non-Interferometric Wide-Field Optical Profilometer (NIWOP)

Figure 1 shows the setup of the NIWOP used in the present work. The light source is a stabilized mercury-xenon lamp. We use an interference filter of 10-nm bandwidth, centered at 365 nm (i-line), to pick up the illuminating wavelength. When the power stabilizer is working, power fluctuation at this wavelength is smaller than 0.5%. A diffuser in the illuminating path is to reduce the effect of spatial fluctuations of the lamp arc. The illuminating optical power on the sample surface is about $20 \mu\text{W}$. A 25 cycles/mm grid pattern made by coating chromium stripes on a fused-silica window is projected onto the sample as the synthesized aperture to produce the optical sectioning. The spatial frequency of this grid pattern projected onto the sample surface is $1.4 \mu\text{m}^{-1}$. Samples are imaged by a dry objective lens of a 0.95 NA, of which the Rayleigh resolution limit is 234 nm. The objective lens can be moved along the optical axis by a PZT-driven mount (P-721.10, Physik Instrumente, Waldbronn, Germany) with a 10-nm smallest step size and 0.04% positioning repeatability. Image magnification is controlled by the lenses between the objective lens and the CCD camera. At the magnification for optimal contrast, the field of view is $18 \times 13 \mu\text{m}$ and the pixel size of images is 25 nm. A pixel size much smaller than the optical resolution provides oversampling, which is a necessary condition for super-resolution image restoration (Carrington et al., 1995). A 14-bit CCD camera cooled at -25°C is used to capture the images.

The details of operation and calibration of a NIWOP can be found in our previous article (Lee et al., 2002). In brief, we take three images with the grid pattern at different spatial phases, and then use the homodyne detection principle to remove the grid pattern and obtain optically sectioned images (Neil et al., 1997). With an adequate setup for the optimal optical sectioning ability, the slope at the linear region of the axial response curve is very sharp, and hence the change of height can be accurately determined as the sample surface is placed slightly away from the focal plane (into the linear region). This topographic sensitivity is employed as the contrast mechanism for the following super-resolution image restoration.

Figure 2 shows a typical response curve in the linear region obtained by the setup in Figure 1 when scanning a reflective mirror along the optical axis. Every data point represents the integral intensity of an image accumulated for 3 seconds. The slope of this linear curve is about $2.5 \mu\text{m}^{-1}$, corresponding to a 1% change in signal intensity when the sample height is displaced by 4 nm. For features with lateral sizes smaller than a wavelength, the sensitivity on topography is reduced; therefore, longer signal accumulation time may be required for an acceptable signal-to-noise ratio.

Image Restoration

The image restoration process is similar to that used in super-resolution DCM (Lee et al., 2003). The iteration kernel of the restoration is an expectation-maximization maximum likelihood estimation (EM-MLE) algorithm of the following form (van Kempen et al., 1996):

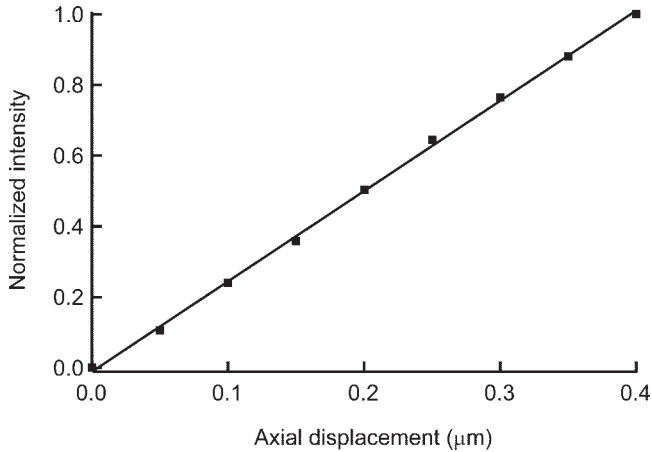


Fig. 2. Linear region of the axial response curve of NIWOP. The slope is about $2.5 \mu\text{m}^{-1}$.

$$\hat{f}^{k+1}(x) = \hat{f}^k(x) \int_y \left[\frac{g(y)}{\int_x h(y-x)\hat{f}^k(x)dx} \right] h(x-y)dy, \quad (1)$$

where f is the estimated object, g is the measured image, h is the PSF of the optical setup, k is the iteration number, x and y represent the coordination of the object and image spaces respectively. The super-resolution capability of MLE algorithms was proposed over a decade ago (Holmes, 1988) and has been experimentally verified. For example, using 50-nm gold beads as the specimen, the lateral extend of the PSF was reduced by a factor of 3.6 after the MLE restoration (Schrader et al., 1996). A detailed frequency-domain analysis of the EM-MLE algorithm showed that fre-

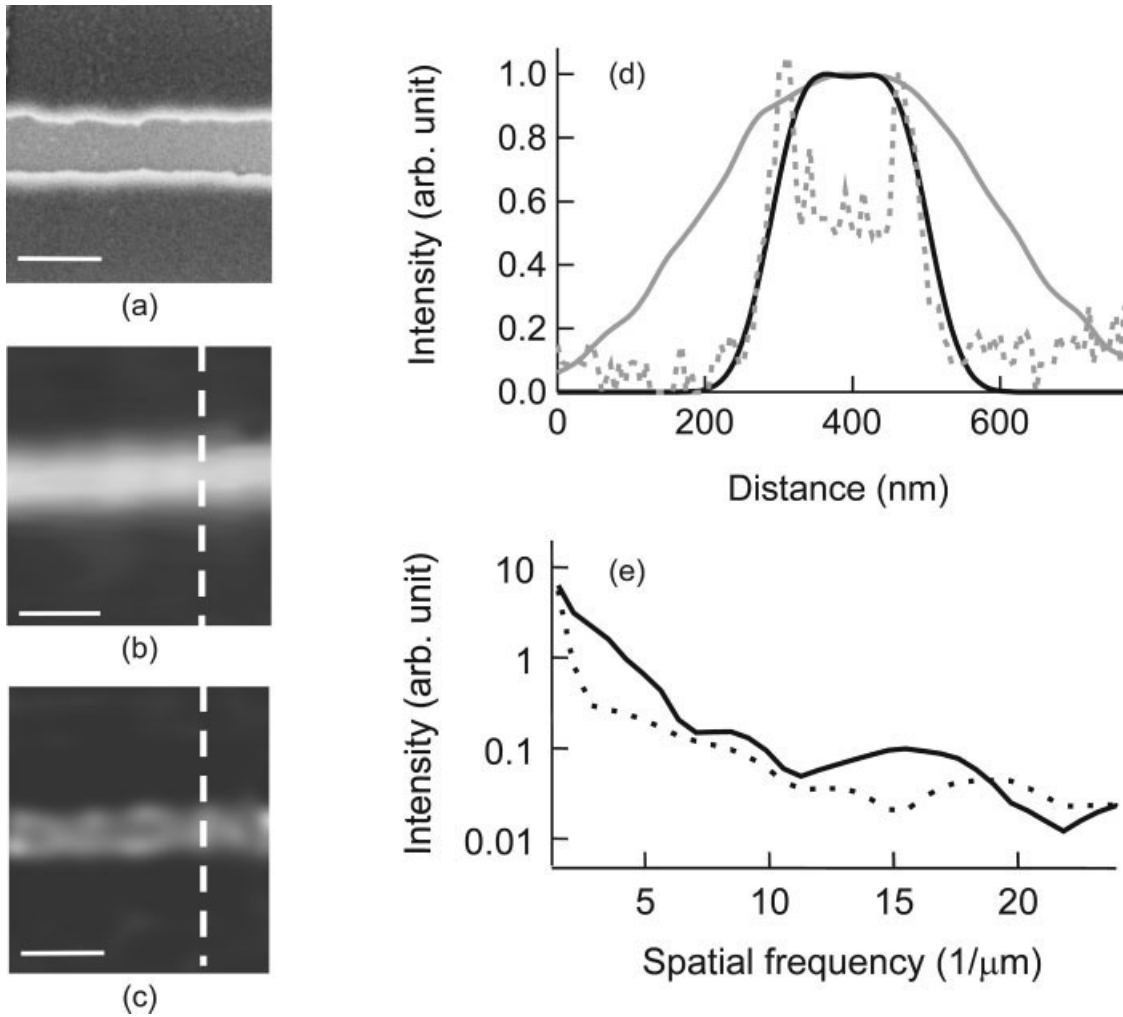


Fig. 3. Images and spectra of a 200-nm-wide, 100-nm-thick chromium line. Scale bars: 365 nm (the working wavelength of NIWOP). **a:** SEM image. **b:** The raw image obtained by NIWOP. The original image size is 44×40 pixels, and we resample it to 132×120 pixels for a better image quality. **c:** Restored NIWOP image. **d:** Gray curve, the profile indicated by the dashed line in **b**. Black curve, the profile

indicated in **c**. For comparison, we also show the profile obtained by SEM as the dashed gray curve. The peaks on the borders of the SEM profile are caused by strong electron scattering of the sharp edges. **e:** Solid line, the signal spectrum in **b**. Dashed line, the noise spectrum. Noise is higher than signal for spatial frequency larger than $18.7 \mu\text{m}^{-1}$.

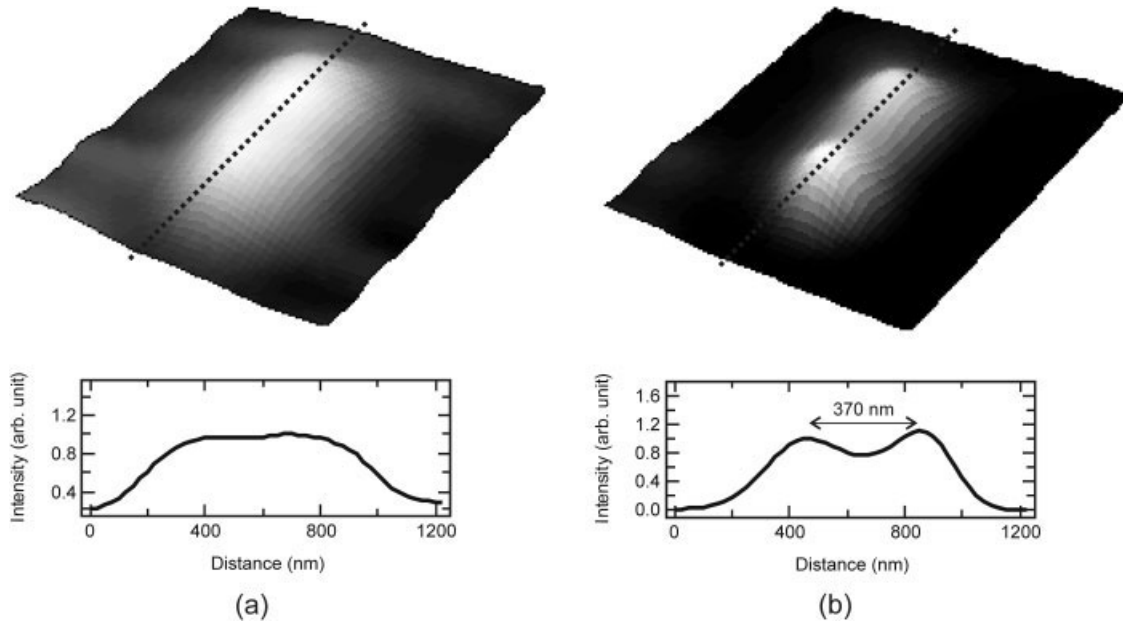


Fig. 4. Surface plot and profile of two 300-nm beads attaching to each other. **a:** The raw NIWOP image and profile along the dashed line. The raw image is resampled from 50×50 pixels to 100×100 pixels before the restoration. **b:** Restored NIWOP image after 750 iterations and profile along the dashed line.

quency components outside the original optical transfer function were recovered with the iterations (Conchello, 1998). This band-extrapolation feature also confirms the super-resolution capability of the EM-MLE restoration.

In addition to super-resolution, the EM-MLE algorithm is more suitable for the NIWOP because the background intensity is significant in the raw topographic images, especially for the samples with height close to the detection limit of the NIWOP. Compared with other deconvolution methods, statistical image restorations like the EM-MLE can restore the degradation of such images owing to low signal-to-noise ratios more effectively (McNally et al., 1999). Moreover, the EM-MLE algorithms are easy to implement, stable for iterations, and able to converge to a global maximum likelihood (Markham and Conchello, 2001). However, when the noise level is high, the convergence of iterations can be severely slowed down because of the noise-amplification effect (Snyder and Miller, 1991). Therefore, additional regulation techniques are required for images with small signal-to-noise ratios. We improve the convergence by monitoring the change of each pixel value between two successive iterations. When the change is larger than a threshold value determined by the signal-to-noise ratio, the restoration program gives up modifying that pixel. This regulation technique has been widely employed in commercial image-processing software products, e.g., MATLAB (The MathWorks, Inc., Natick, MA). The restored image is evaluated by the I -divergence difference measure (Csiszar, 1991). In the following restorations, we set the iteration numbers such that the I -divergence measures approach 10^{-3} .

RESULTS AND DISCUSSION

Because the restoration process and the final image resolution are both determined by the signal-to-noise ratio, we first use a 200-nm-wide, 100-nm-high chromium stripe coated on glass to check the signal quality of raw images. We coat the whole surface with 50-nm gold for uniform reflectivity. Owing to the lack of contrast, the stripe is almost invisible with ordinary bright-field optical microscopy. Figure 3a shows the scanning electron microscope (SEM) image of this sample. With the topographic sensitivity of NIWOP, we obtain the optical image in Figure 3b. The exposure time for each frame of one sectioned image is 3 seconds. In the raw images, the measured intensity of the stripe is 50–70% the dynamic range of the CCD camera. Owing to the low resolution of this raw image, it is impossible to guarantee that the imaged positions of Figure 3a and b are exactly the same. But from the observation by SEM, we know that the width of this stripe is uniform. Figure 3c is the super-resolution image after 1,500 iterations. The line profiles at the position indicated by the dashed lines are compared in Figure 3d. The width of 10–90% the edge response is equivalent to the full width at half maximum of the PSF. Therefore, from the edge responses we estimate that the lateral resolution is improved from 230 to 70 nm. The best lateral resolution achievable by the MLE restoration is limited by the signal-to-noise ratio. Based on the analysis by Snyder et al. (1987), a “crossover” point in the spectra of the signal and noise sets the limit of lateral resolution after the MLE restoration (Snyder et al., 1987). Figure 3e shows the spectra of signal and noise in Figure 3b. The crossover frequency

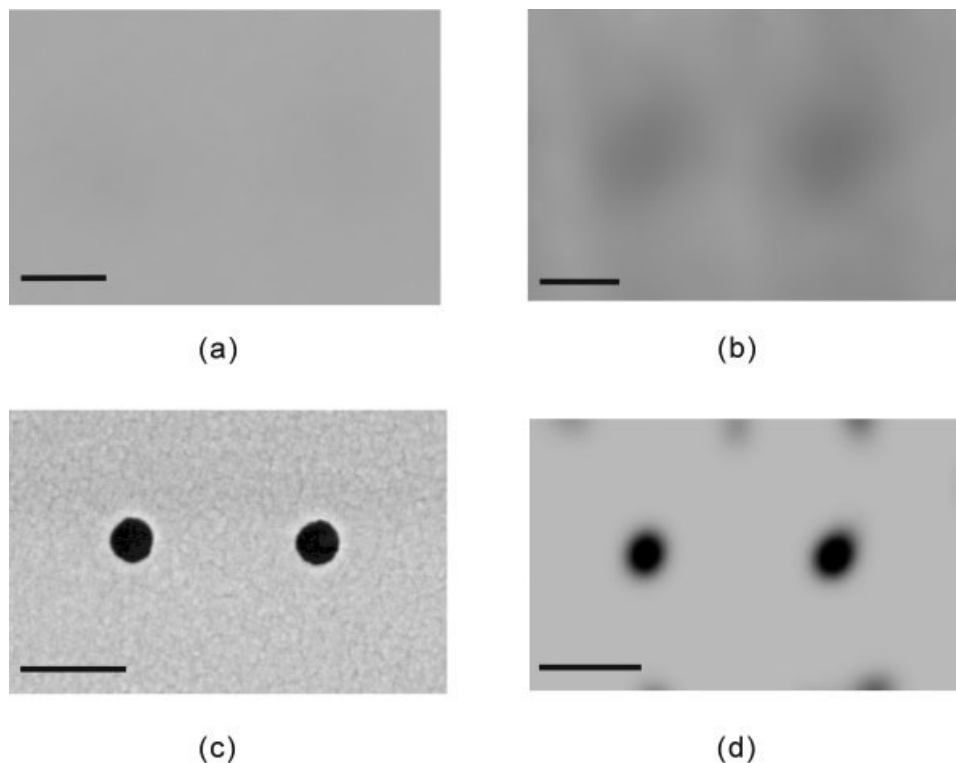


Fig. 5. Images of two 100-nm holes drilled on PMMA photoresist. Scale bars = 365 nm. **a:** Bright-field image. **b:** The raw image obtained by NIWOP. We resample it from 50×33 pixels to 200×132 pixels before the restoration. **c:** SEM image. **d:** Restored NIWOP image after 750 iterations.

is found to be $18.7 \mu\text{m}^{-1}$, equivalent to a lateral distance of 53 nm (about $\lambda/7$).

Figure 4 shows images of two latex beads (LB-3, Sigma Chemical Co., St. Louis, MO) on glass, attaching to each other. The original diameters of these beads are about 300 nm. We coated the whole surface with 100 nm gold for uniform reflectivity. Surface plots are used here for a clearer comparison. Figure 4a is the raw NIWOP image and profile. Because of diffraction, we cannot determine the position and shape of the beads in the raw image. After the restoration, we obtain a super-resolution image and profile as shown in Figure 4b. The profile shows an evident improvement on the resolution. The distance between the peaks of the restored profile is 370 nm, while the distance between the centers of the two beads measured by SEM is 340 nm. The 30-nm difference implies the accuracy for distance determination on the restored images.

In order to demonstrate the imaging capability of this technique on features of reverse contrast such as holes and pits on a flat surface, we use electron beams to write solid circles on poly-methylmethacrylate (PMMA) photoresist and then develop them to form holes on the surface. The holes are of 100 nm diameter and 200 nm depth. Figure 5a shows the bright-field image, and Figure 5b is the NIWOP image with much better contrast. Figure 5c is the SEM image and Figure 5d is the restored image of Figure 5b. Although a few false images of these holes at the edges are generated during the restoration process, the holes themselves

are clearly resolved, and the image quality is close to that of the SEM counterpart.

CONCLUSION

In conclusion, we have demonstrated super-resolution bright-field imaging by using an EM-MLE algorithm to restore the images from a non-interferometric wide-field optical profilometer with nanometer topographic contrast. With the i-line (365 nm) emission from a mercury-xenon lamp as the light source of power fluctuation smaller than 0.5%, the noise is smaller than signal for spatial frequency lower than $18.7 \mu\text{m}^{-1}$. Therefore, the highest lateral resolution after the restoration can achieve 53 nm, or about $\lambda/7$. In addition to characterizing a 200-nm-wide, 100-nm-thick chromium stripe, we also use this technique to observe 300-nm beads on glass and 100-nm holes drilled on PMMA photoresist. For these observations, the image acquisition time for a complete frame is less than 10 seconds. The current imaging speed is limited by the long exposure time required for a high signal-to-noise ratio. If a brighter ultraviolet light source is employed to illuminate the sample, the image acquisition time can be shortened and real-time capture would be possible. After the restoration process, dynamic morphological changes can then be displayed on continuous super-resolution frames. We believe this method can serve as a powerful tool for monitoring the dynamical phenomena in the nanoscale.

REFERENCES

- Akduman I, Brand U, Grochmalicki J, Hester G, Pike R, Bertero M. 1998. Superresolving masks for incoherent high-numerical-aperture scanning microscopy in three dimensions. *J Opt Soc Am A* 15:2275–2287.
- Barty A, Nugent KA, Paganin D, Roberts A. 1998. Quantitative optical phase microscopy. *Opt Lett* 23:817–819.
- Carrington WA, Lynch RM, Moore EDW, Isenberg G, Fogarty KE, Fay FS. 1995. Superresolution three-dimensional images of fluorescence in cells with minimal light exposure. *Science* 268:1483–1486.
- Conchello J-A. 1998. Superresolution and convergence properties of the expectation-maximization algorithm for maximum-likelihood deconvolution of incoherent images. *J Opt Soc Am A* 15:2609–2619.
- Csiszar I. 1991. Why least squares and maximum entropy? An axiomatic approach to inverse problems. *Annu Stat* 19:2032–2066.
- Frohn JT, Knapp HF, Stemmer A. 2000. True optical resolution beyond the Rayleigh limit achieved by standing wave illumination. *Proc Natl Acad Sci USA* 97:7232–7236.
- Gustafsson MGL. 2000. Surpassing the lateral resolution limit by a factor of two using structured illumination microscopy. *J Microsc* 198:82–87.
- Holmes TJ. 1988. Maximum-likelihood image restoration adapted for noncoherent optical imaging. *J Opt Soc Am A* 5:666–673.
- Klar TA, Hell SW. 1999. Sub-diffraction resolution in far-field fluorescence microscopy. *Opt Lett* 24:954–956.
- Lee C-H, Wang J. 1997. Non-interferometric differential confocal microscopy with 2-nm depth resolution. *Opt Commun* 135:233–237.
- Lee C-H, Mong H-Y, Lin W-C. 2002. Non-interferometric wide-field optical profilometry with nanometer depth resolution. *Opt Lett* 27:1773–1775.
- Lee C-H, Chiang H-Y, Mong H-Y. 2003. Sub-diffraction-limit imaging based on the topographic contrast of differential confocal microscopy. *Opt Lett* 28:1772–1774.
- Markham J, Conchello J-A. 2001. Fast maximum-likelihood image-restoration algorithms for three-dimensional fluorescence microscopy. *J Opt Soc Am A* 18:1062–1071.
- McNally JG, Karpova T, Cooper J, Conchello J-A. 1999. Three-dimensional imaging by deconvolution microscopy. *Methods* 19:373–385.
- Neil MAA, Juskaitis R, Wilson T. 1997. Method of obtaining optical sectioning by using structured light in a conventional microscope. *Opt Lett* 22:1905–1907.
- Schrader M, Hell SW, van der Voort HTM. 1996. Potential of confocal microscopes to resolve in the 50–100 nm range. *Appl Phys Lett* 69:3644–3646.
- Snyder DL, Miller MI. 1991. Random point processes in time and space. New York: Springer-Verlag.
- Snyder DL, Miller MI, Thomas LJ Jr., Polite DG. 1987. Noise and edge artifacts in maximum-likelihood reconstructions for emission tomography. *IEEE Trans Med Imag* 6:228–235.
- Tsai C-W, Lee C-H, Wang J. 1999. Deconvolution of local surface response from topography in nanometer profilometry with a dual-scan method. *Opt Lett* 24:1732–1734.
- van Kempen GMP, van der Voort HTM, Bauman JGJ, Strasters KC. 1996. Comparing maximum likelihood estimation and constrained Tikhonov-Miller restoration. *IEEE Eng Med Biol* 15:76–83.
- Walker JG, Pike ER, Davies RE, Young MR, Brakenhoff GJ, Bertero M. 1993. Superresolving scanning optical microscopy using holographic optical processing. *J Opt Soc Am A* 10:59–64.